01 Mar 1975

Differential Cross Sections for Elastic and Inelastic Scattering of 15-100-keV Li^+ by He

John T. Park
Missouri University of Science and Technology, parkj@mst.edu

Victor Pol

James E. Lawler

Jacob M. George

et. al. For a complete list of authors, see https://scholarsmine.mst.edu/phys_facwork/1356

Recommended Citation

J. T. Park et al., "Differential Cross Sections for Elastic and Inelastic Scattering of 15-100-keV Li^+ by He," *Physical Review A*, vol. 11, no. 3, pp. 857-864, American Physical Society (APS), Mar 1975.
The definitive version is available at https://doi.org/10.1103/PhysRevA.11.857

Differential cross sections for elastic and inelastic scattering of 15–100-keV Li^+ by He†

J. T. Park, V. Pol,* J. Lawler,‡ J. George, J. Aldag, J. Parker,‡ and J. L. Peacher
Physics Department, University of Missouri-Rolla, Rolla, Missouri 65401
(Received 29 October 1974)

Sets of energy-loss spectra for Li^+ incident on He that were taken at a series of scattering angles were used to calculate differential cross sections. Differential cross sections are given for elastic scattering and for excitation of the He ($n = 2$) states. The differential cross section is also given for excitation of states corresponding to a 60-eV energy loss. These inelastic differential cross sections exhibit maxima at scattering angles greater than zero. The velocity dependence of the cross sections can be compensated by displaying the elastic data in ρ-vs-τ plots and the inelastic data in ρ-vs-$E^{3/2}\theta$ plots. When displayed in terms of these variables, the data are strikingly similar to those reported for $Li^+ + He$ collisions at much lower impact energies.

INTRODUCTION

The $Li^+ + He$ collision makes it possible to study one of the simplest ion-atom collisions. The collision involves the most straightforward interaction of two complete K shells. The interaction is free from perturbations from outer-shell electrons. The Li^+ core is bound tight enough so that it is unexcited in the collisions.

The $Li^+ + He$ collision exhibits several interesting characteristics. The $Li^+ + He$ excitation cross sections are weakly dependent on the scattering angle in comparison with the $He^+ + He$ cross sections. The angular dependence of the differential cross sections for $Li^+ + He$ collisions is consistent with a curve-crossing mechanism for excitation. Possible excitation mechanisms are suggested by the correlation diagrams that have been constructed by using the electron-promotion model, which includes rotational coupling.[1-3] The excitation processes are understood in terms of the diabatic correlation of the $(\sigma_a 1s)^2(\sigma_b 1s)^2\ ^1\Sigma$ state of $LiHe^+$ to the $(1s\sigma)^2(2p\sigma)^2\ ^1\Sigma$ state, followed by rotational coupling to the $(1s\sigma)^2(2p\sigma 2p\pi)^1\Pi$ and the $(1s\sigma)^2(2p\pi)^2\ ^1\Delta$ states of $LiHe^+$. The coupling of the $^1\Sigma$ state to the $^1\Pi$ state leads to the excitation of the $He(1s2p)^1P$ state and to a charge-exchange process. The coupling of the $^1\Sigma$ state to the $^1\Delta$ state leads to the excitation of the $He(2p^2)^1D$ state and to another charge exchange process. An examination of the energy-loss spectra for Li^+ incident on a He target shows that the spectra are dominated by transitions involving energy losses of 20 and 60 eV. Francois *et al.*[3] found that the branching ratio between the excitation and charge-exchange process did not depend on the scattering angle. This condition indicates that the primary excitation mechanism for both processes is the same. Park *et al.*[4] noted that the $He(1s2s)^1S$ state is excited as well as the $He(1s2p)^1P$ state. This excitation can be explained as a mixing, after the primary excitation process, of the states at large internuclear distances. This explanation is consistent with the observation that the branching ratio for the $He(1s2s)^1S$ and $He(1s2p)^1P$ excitations is independent of the scattering angle.

The current set of measurements extends the energy range over which the $Li^+ + He$ collision has been studied to 100 keV. Differential cross sections are now available from 1 to 100 keV.

APPARATUS

The apparatus and the general method, which is employed in measuring differential cross sections, have been discussed in detail elsewhere.[5-8] In the current experiment, lithium ions, which are produced in a hot-surface-emission source,[9] are mass analyzed with a Wien filter. Selected ions are then accelerated and passed first through two pairs of deflection plates and then through an entrance collimator into a chamber containing the target gas. After the ions have traversed a scattering chamber, they travel through an exit collimator. After collimation the ions are magnetically analyzed to remove any products of charge-changing collisions. When the ions enter the decelerator, they are decelerated to 2000.00 V and analyzed with a 127° electrostatic analyzer. Energy-loss spectra are obtained by increasing the difference between the potentials of the accelerator terminal and the decelerator terminal. Whenever the increased potential-energy compensates for a discrete energy loss in the projectile-target system, a peak is detected in the spectrum. The energy-loss scale can be determined to an accuracy of ± 0.03 eV.[10]

Measurements of the differential cross sections involve a series of energy-loss spectra, which are obtained by using the above technique. The angle at which the ions enter the target chamber is varied by changing the entrance collimator

angle θ and adjusting the voltages on the two pairs of deflection plates that precede the collimator. At a given setting of the collimator, the deflection voltages are adjusted to reproduce the initial beam current at the center of the scattering chamber. The series of spectra obtained at various scattering angles can then be used to determine differential cross sections. In the case of the 60-eV peak, the signal produced by the excitation is superimposed on the background signal that is produced by the target ionization continuum. The current resulting from this process is calculated by first fitting the background on either side of the peak to a quadratic function and then subtracting the integral of this function from the total integral over the region of the peak.

The differential cross section for a particular process can be determined from the following equation[7]:

$$\Delta\sigma_p(\theta)/\Delta\Omega = [I_{1p}(\theta)]_f/(I_{10})_f nL\Delta\Omega\,, \qquad (1)$$

in which $[I_{1p}(\theta)]_f$ is the final current that results from singly charged particles that have lost energy in the interaction, p, and have been scattered into the solid angle, $\Delta\Omega$, at the angle θ. The term $(I_{10})_f$ represents the final current produced by the integration of the elastic beam over all angles. The target gas density is n and the length of the interaction region is L. Equation (1) gives the differential cross section $d\sigma(\theta)/d\Omega$ averaged over the interval from $\theta - \frac{1}{2}\Delta\theta$ to $\theta + \frac{1}{2}\Delta\theta$, in which $\Delta\theta$ is the effective angular resolution of the apparatus. The errors associated with making the approximation required by the finite sizes of the measuring devices have been discussed in detail by Pol *et al.*[5] The way in which the apparatus is designed and the extremely small angles involved minimize the variations of L and $\Delta\Omega$ with angle. The small scattering angles, however, result in a rather large uncertainty in θ and $\Delta\Omega$.[5]

The angular divergence of the beam entering the scattering chamber, and the angular acceptance and angular detection efficiency of the decelerator-detector system can be measured independently. However, because the angular distribution of the beam in the collision region cannot be measured accurately, no attempt was made to deconvolute the data. The convolution of the acceptance angle of the detector with the divergence of the incident beam is obtained by plotting the current detected in the analyzer as a function of incident-beam angle when there is no gas in the collision cell. The measurement is consistent with values of the convolution of the angular acceptance and beam divergence and hence is used as the effective angular resolution $\Delta\theta$.

DATA

A set of energy-loss spectra for 25-keV Li^+ incident on He is shown in Fig. 1. The energy resolution is ≈ 0.8 eV. The first (zero-energy-loss) peak at each angle corresponds to the initial beam or to particles that have been elastically scattered. All of the data for ions scattered at an angle show an elastic energy loss. The inelastic losses are determined after first correcting for the elastic energy losses. The peak at 21-eV energy loss is due to particles which have undergone discrete energy losses to the He ($n=2$) states. This peak contains contributions either from ions, which caused excitation of the He(2^1S) or from ions

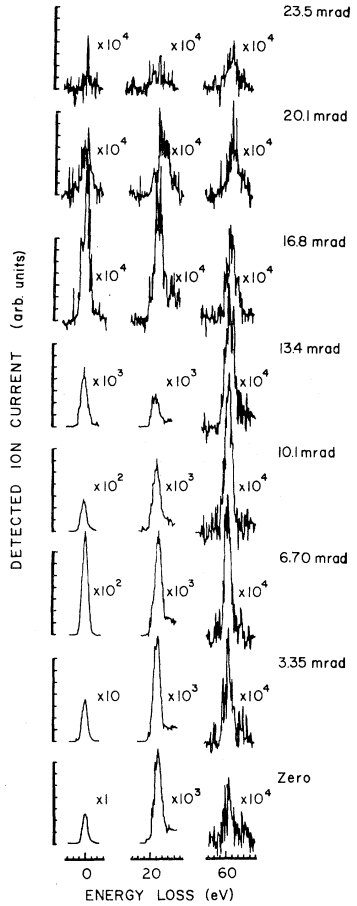

FIG. 1. Energy-loss spectra showing the elastic 20-eV energy-loss and 60-eV energy-loss peaks of the Li^+ + He spectrum at various center-of-mass scattering angles for 25-keV Li^+ ions incident on He. These are reproductions of recorder output traces. The data actually used in data analysis were taken in digital form for computer analysis.

which excited the He(2^1P) state. Ions, which excited the He(2^1S) and those which excited the He(2^1P) state are present at all scattering angles where the ion intensity permits measurements.[4]

Excitation of the triplet states of He would require a spin flip of an electron in both the He and Li^+ K shells if spin is to be conserved. Simultaneous excitation of He and Li^+ would result in an energy loss of ≈ 79 eV. Structure is not detected at or near 79-eV energy loss.

A limitation to the applicability of Eq. (1) is the possibility of multiple collisions involving one inelastic collision and one or more elastic collisions. In this case, there could be a contribution to $[I_{1p}(\theta)]_f$ from particles which have been scattered several times, leading to an ambiguity in the scattering angle of the energy-loss process. Under "single-collision" conditions, the equation is exact[7]; however, it is difficult to define single-collision conditions for elastic scattering, because multiple collisions through very small angles cannot be separated from the incident beam. Multiple inelastic scattering would produce peaks in the energy-loss spectrum at 42, 81, or 120 eV. Structure is not observed at any of these energy losses. Because for many scattering angles the elastic and inelastic differential cross sections are of almost the same magnitude, the probability of the occurrence of multiple inelastic collisions and of multiple elastic collisions is approximately equal. The absence of multiple inelastic peaks in the spectrum indicates that multiple elastic scattering does not significantly affect the reported cross sections.

The 60-eV peak can contain contributions from ions which have excited the He($2s^2$)^1S state at 57.8 eV, the He($2s2p$)^1P state at 60 eV, or the He($2p^2$)^1D state at 60 eV. Ions, which have excited the He($2p^2$)^1S state at 62.1 eV, can also contribute to this peak. Several possible excitations of Li^+ also involve energy losses of about 60 eV. Excitations of $Li^+(1s2s)^1S$ and $Li^+(1s2p)^1P$ states, which require energy losses of 60.8 and 62.2 eV, can be allowed without requiring a simultaneous spin flip on the part of the incident Li^+ and the helium target. The $Li^+(1s2p)^1P$ state can be expected to be the more easily excited of the two states. The peak's location indicates that either the He($2s2p$)^1P or the He($2p^2$)^1D state or both is probably the dominant excitation product. The excitation of He($2p^2$)^1D is the most probable if the electron-promotion model is followed, but it cannot be established by the experiment whether it is the only excited state.

Data obtained from sets of spectra similar to those in Fig. 1 are tabulated in Table I. Standard deviations of the cross sections are also given in the table. The $\Delta\theta$ represents the angular resolution. It represents an estimate, which was arrived at by using all available data on the angular divergence of the beam, the angular resolution of the decelerator-analyzer system, and the angular dependence of the detected current that was observed when there was no gas in the chamber.

The individual contributions of the He(2^1S) and He(2^1P) excitations were reported by Park *et al.*[4] The He(2^1S) excitation represents $(38 \pm 11)\%$ of the 21-eV peak.[4] This fraction appears to be constant within the uncertainties involved and to be independent of both energy and angle. The observed fluctuations are consistent with the uncertainties in the measurements. The value of the cross sections for the He(2^1S) and He(2^1P) excitations can be obtained by multiplying the values for the 21-eV peak in Table I by 38 and 62%, respectively and including the additional uncertainties.

Systematic errors for this apparatus have been discussed by Pol *et al.*[5] The estimated errors are 5% in the pressure measurement, 1% in effective collision length, and 0.5% in target temperature. The largest error is due to the uncertainties in the angular resolution. This uncertainty affects I_{1p} and I_{10}. The effect of uncertainties in angular resolution on the cross sections is not as large as the uncertainty in the angular resolution itself, because the error is partially canceled in taking the ratio that is involved in calculating the cross sections. The error, which results from uncertainties in the angular resolution is believed to be less than 30%. The total systematic error in the cross sections is estimated to be less than 42%. The scattering angle θ has a possible systematic error of 1.5×10^{-4} rad (c.m.), which results from errors made in the measurements. The fact that the cross sections are averaged over the angular resolution and are possibly smeared by elastic scattering must be remembered when the shapes of their curves are analyzed. By using Molieres's theory of multiple scattering,[11] an estimate of the "effective number of collisions" can be made. This estimate indicates that even in the case of elastic scattering the contribution to the observed cross section, which results from multiple scattering, is very small. This is probably true for the inelastic cross sections; however, the elastic cross sections fall off very rapidly with the magnitude of the angle. As a result, a very small amount of multiple scattering probably could affect the large-angle scattering. This could produce a slight upward curvature in the elastic differential cross sections when the scattering angles are large.

TABLE I. Average differential cross sections $(d\sigma/d\Omega)_{av}$ (c.m.), for the elastic and inelastic peaks in the $Li^+ + He$ energy-loss spectrum. Limits on the data indicate standard deviations in the data.

θ (c.m.) (10^{-3} rad)	Elastic peak (cm^2/sr)	20-eV peak (cm^2/sr)	60-eV peak (cm^2/sr)
	Incident energy = 15 keV (lab) $\Delta\theta = 7\times10^{-4}$ rad		
0		$(2.8\pm1)\times10^{-15}$	$(3\pm30)\times10^{-17}$
2		$(3.4\pm1.2)\times10^{-15}$	$(2\pm30)\times10^{-17}$
4	$(5.7\pm0.9)\times10^{-13}$	$(4.2\pm1.8)\times10^{-15}$	$(3\pm30)\times10^{-17}$
6	$(2.8\pm0.4)\times10^{-13}$	$(5.5\pm2.1)\times10^{-15}$	$(3\pm3)\times10^{-16}$
8	$(1.6\pm0.2)\times10^{-13}$	$(6.1\pm2.4)\times10^{-15}$	$(9.6\pm5)\times10^{-16}$
10	$(9.7\pm1.5)\times10^{-14}$	$(6.3\pm2.4)\times10^{-15}$	$(1.3\pm0.7)\times10^{-15}$
12	$(6.6\pm1.0)\times10^{-14}$	$(6.2\pm2.4)\times10^{-15}$	$(1.1\pm0.7)\times10^{-15}$
14	$(4.3\pm0.7)\times10^{-14}$	$(5.9\pm2.8)\times10^{-15}$	$(1.1\pm0.6)\times10^{-15}$
16	$(2.7\pm0.4)\times10^{-14}$	$(4.9\pm2.4)\times10^{-15}$	$(1.1\pm0.6)\times10^{-15}$
18	$(1.7\pm0.3)\times10^{-14}$	$(4.1\pm2.2)\times10^{-15}$	$(1.1\pm0.7)\times10^{-15}$
20	$(1.1\pm0.3)\times10^{-14}$	$(3.7\pm2.2)\times10^{-15}$	$(9.2\pm5.0)\times10^{-16}$
22	$(6.5\pm1.0)\times10^{-15}$	$(3.1\pm2.1)\times10^{-15}$	$(6.5\pm3.0)\times10^{-16}$
24	$(3.9\pm0.6)\times10^{-15}$	$(2.4\pm2.0)\times10^{-15}$	$(3.4\pm2)\times10^{-16}$
26	$(2.7\pm0.6)\times10^{-15}$	$(1.7\pm1.9)\times10^{-15}$	$(3.1\pm2)\times10^{-16}$
28	$(2.0\pm0.6)\times10^{-15}$	$(1.0\pm1.0)\times10^{-15}$	
30	$(1.7\pm0.6)\times10^{-15}$	$(5.8\pm4)\times10^{-16}$	
	Incident energy = 20 keV (lab) $\Delta\theta = 9\times10^{-4}$ rad		
0		$(1.1\pm0.6)\times10^{-14}$	$(3.0\pm3.0)\times10^{-16}$
2		$(1.2\pm0.4)\times10^{-14}$	$(5.4\pm3.0)\times10^{-16}$
4	$(5.9\pm0.9)\times10^{-13}$	$(1.3\pm0.4)\times10^{-14}$	$(5.5\pm3.0)\times10^{-16}$
6	$(2.6\pm0.5)\times10^{-13}$	$(1.3\pm0.4)\times10^{-14}$	$(6.6\pm4.0)\times10^{-16}$
8	$(1.3\pm0.3)\times10^{-13}$	$(1.2\pm0.4)\times10^{-14}$	$(1.3\pm1.0)\times10^{-15}$
10	$(7.1\pm0.9)\times10^{-14}$	$(1.2\pm0.5)\times10^{-14}$	$(2.1\pm1.5)\times10^{-15}$
12	$(3.8\pm0.6)\times10^{-14}$	$(9.8\pm2.0)\times10^{-15}$	$(2.2\pm1.3)\times10^{-15}$
14	$(2.2\pm0.4)\times10^{-14}$	$(8.4\pm1.7)\times10^{-15}$	$(2.3\pm1.0)\times10^{-15}$
16	$(1.1\pm0.3)\times10^{-14}$	$(6.3\pm2.3)\times10^{-15}$	$(2.4\pm1.2)\times10^{-15}$
18	$(5.5\pm1.3)\times10^{-15}$	$(4.3\pm1.9)\times10^{-15}$	$(2.3\pm1.2)\times10^{-15}$
20	$(2.9\pm0.7)\times10^{-15}$	$(2.8\pm1.6)\times10^{-15}$	$(2.0\pm1.3)\times10^{-15}$
22	$(1.6\pm1.6)\times10^{-15}$	$(1.4\pm1.3)\times10^{-15}$	$(1.9\pm1.7)\times10^{-15}$
	Incident energy = 25 keV (lab) $\Delta\theta = 1\times10^{-3}$ rad		
0		$(1.78\pm0.4)\times10^{-14}$	$(1.0\pm0.5)\times10^{-15}$
2		$(1.81\pm0.4)\times10^{-14}$	$(1.1\pm0.4)\times10^{-15}$
4	$(5.9\pm1.2)\times10^{-13}$	$(2.02\pm0.4)\times10^{-14}$	$(1.5\pm0.5)\times10^{-15}$
6	$(2.3\pm0.5)\times10^{-13}$	$(1.88\pm0.4)\times10^{-14}$	$(1.76\pm0.5)\times10^{-15}$
8	$(9.2\pm2.1)\times10^{-14}$	$(1.59\pm0.4)\times10^{-14}$	$(2.05\pm0.5)\times10^{-15}$
10	$(3.8\pm1.0)\times10^{-14}$	$(1.2\pm0.5)\times10^{-14}$	$(2.35\pm0.5)\times10^{-15}$
12	$(1.7\pm0.5)\times10^{-14}$	$(8.2\pm2.6)\times10^{-15}$	$(2.36\pm0.5)\times10^{-15}$
14	$(6.5\pm2.3)\times10^{-15}$	$(4.9\pm2.0)\times10^{-15}$	$(2.1\pm0.6)\times10^{-15}$
16	$(3.2\pm1.3)\times10^{-15}$	$(3.1\pm0.9)\times10^{-15}$	$(1.8\pm0.7)\times10^{-15}$
18	$(1.8\pm0.8)\times10^{-15}$	$(2.0\pm1.0)\times10^{-15}$	$(1.6\pm1.0)\times10^{-15}$
20	$(1.2\pm0.9)\times10^{-15}$	$(1.2\pm1.0)\times10^{-15}$	$(1.3\pm1.0)\times10^{-15}$
22		$(9.0\pm5.0)\times10^{-16}$	
24		$(6.1\pm5.0)\times10^{-16}$	
	Incident energy = 30 keV (lab) $\Delta\theta = 1\times10^{-3}$ rad		
0		$(3.9\pm0.9)\times10^{-14}$	$(4.0\pm3.0)\times10^{-15}$
2		$(5.2\pm0.8)\times10^{-14}$	$(2.8\pm2.0)\times10^{-15}$
4	$(9.1\pm1.0)\times10^{-13}$	$(5.0\pm0.8)\times10^{-14}$	$(3.2\pm2.1)\times10^{-15}$
6	$(2.8\pm0.4)\times10^{-13}$	$(3.8\pm0.8)\times10^{-14}$	$(6.5\pm2.4)\times10^{-15}$
8	$(8.6\pm1.0)\times10^{-14}$	$(2.5\pm0.6)\times10^{-14}$	$(8.0\pm2.6)\times10^{-15}$
10	$(2.7\pm0.4)\times10^{-14}$	$(1.4\pm0.6)\times10^{-14}$	$(6.9\pm2.4)\times10^{-15}$
12	$(9.5\pm2.3)\times10^{-15}$	$(8.2\pm2.3)\times10^{-15}$	$(5.5\pm2.1)\times10^{-15}$
14	$(4.0\pm1.0)\times10^{-15}$	$(4.3\pm1.2)\times10^{-15}$	$(4.3\pm1.9)\times10^{-15}$
16	$(2.0\pm1.0)\times10^{-15}$	$(1.9\pm1.0)\times10^{-15}$	$(3.3\pm2.7)\times10^{-15}$

Table I (continued)

θ(c.m.) (10^{-3} rad)	Elastic peak (cm^2/sr)	20-eV peak (cm^2/sr)	60-eV peak (cm^2/sr)
	Incident energy = 40 keV (lab) $\Delta\theta = 1.3\times10^{-3}$ rad		
0		$(9.3\pm4.9)\times10^{-14}$	$(2.3\pm1.3)\times10^{-15}$
2		$(7.8\pm2.7)\times10^{-14}$	$(4.5\pm2.5)\times10^{-15}$
4	$(5.7\pm2.3)\times10^{-13}$	$(5.6\pm2.7)\times10^{-14}$	$(6.4\pm3.6)\times10^{-15}$
6	$(1.3\pm0.4)\times10^{-13}$	$(3.3\pm1.6)\times10^{-14}$	$(6.6\pm3.6)\times10^{-15}$
8	$(3.0\pm0.8)\times10^{-14}$	$(1.6\pm0.8)\times10^{-14}$	$(5.8\pm2.6)\times10^{-15}$
10	$(6.8\pm2.6)\times10^{-15}$	$(6.4\pm3.9)\times10^{-15}$	$(4.5\pm1.8)\times10^{-15}$
12	$(2.1\pm1.4)\times10^{-15}$	$(2.6\pm1.8)\times10^{-15}$	$(3.2\pm1.0)\times10^{-15}$
14	$(8.1\pm3.5)\times10^{-16}$	$(1.2\pm1.0)\times10^{-15}$	$(2.2\pm1.2)\times10^{-15}$
16	$(3.8\pm2.0)\times10^{-16}$	$(5.5\pm3.7)\times10^{-16}$	$(1.3\pm0.8)\times10^{-15}$
	Incident energy = 50 keV (lab) $\Delta\theta = 1.3\times10^{-3}$ rad		
0		$(2.5\pm1.6)\times10^{-13}$	$(2.2\pm1.2)\times10^{-15}$
2		$(1.7\pm0.8)\times10^{-13}$	$(1.1\pm0.6)\times10^{-14}$
4	$(6.6\pm3.1)\times10^{-13}$	$(7.3\pm3.8)\times10^{-14}$	$(1.2\pm0.7)\times10^{-14}$
6	$(4.5\pm3.0)\times10^{-14}$	$(2.1\pm1.4)\times10^{-14}$	$(7.3\pm3.9)\times10^{-15}$
8	$(3.6\pm2.5)\times10^{-15}$	$(5.4\pm3.6)\times10^{-15}$	$(5.9\pm5.5)\times10^{-15}$
10	$(2.7\pm1.7)\times10^{-16}$	$(1.6\pm1.4)\times10^{-15}$	$(2.3\pm2.3)\times10^{-15}$
12	$(2.6\pm3.0)\times10^{-17}$		
	Incident energy = 70 keV (lab) $\Delta\theta = 9\times10^{-4}$ rad		
0		$(3.3\pm1.3)\times10^{-13}$	$(8.5\pm1.9)\times10^{-15}$
2		$(1.5\pm0.5)\times10^{-13}$	$(1.2\pm0.8)\times10^{-14}$
4	$(1.5\pm0.8)\times10^{-13}$	$(3.8\pm1.8)\times10^{-14}$	$(9.5\pm1.0)\times10^{-15}$
6	$(1.35\pm0.7)\times10^{-14}$	$(8.3\pm4.2)\times10^{-15}$	$(5.6\pm1.9)\times10^{-15}$
8	$(2.8\pm2.0)\times10^{-15}$	$(1.8\pm0.9)\times10^{-15}$	$(2.8\pm1.2)\times10^{-15}$
10	$(4.7\pm3.3)\times10^{-16}$	$(1.1\pm0.6)\times10^{-15}$	$(8.2\pm4.1)\times10^{-16}$
	Incident energy = 100 keV (lab) $\Delta\theta = 7\times10^{-4}$ rad		
0		$(4.5\pm1.2)\times10^{-13}$	$(2.7\pm0.8)\times10^{-14}$
2		$(9.1\pm1.3)\times10^{-14}$	$(1.4\pm0.1)\times10^{-14}$
4	$(6.1\pm1.9)\times10^{-14}$	$(1.5\pm0.5)\times10^{-14}$	$(6.9\pm2.6)\times10^{-15}$
6	$(4.9\pm2.6)\times10^{-15}$	$(3.4\pm1.0)\times10^{-15}$	$(3.0\pm1.4)\times10^{-15}$

DISCUSSION

Insofar as is know at this time, there are no cross-section measurements which can be compared with those discussed above. Barat *et al.*[12] obtained energy-loss spectra for 80-keV Li^+ ions by using an acceleration-deceleration technique. Their 4-eV resolution was not adequate to study individual states. Boersch *et al.*[13] also made measurements of energy-loss spectra. They achieved resolutions of 1–2 eV for 30-keV Li^+ ions. They did not resolve the individual states, but their location of the He($n=2$) excitation peak at 20.8 eV is consistent with a sizable contribution from the He($2\,^1S$) state. They also detected an energy-loss peak at 59.3 eV, which they explained as an excitation of the lithium ion. While the results of both of these groups are consistent with observations made in the current study, neither group measured differential cross sections. Other measurements for Li^+ + He collisions that are available were made at much lower energies. The low-energy measurements that were made by Lorents and Conklin[1] were normalized to the theoretical calculation of Catlow *et al.*[14] to obtain absolute cross sections. This theoretical calculation provides a reduced differential scattering cross section $\rho = \theta \sin\theta\, d\sigma/d\Omega$. Lorents and Conklin observed that the sum of their elastic and inelastic differential cross sections fell below the theoretical value for the total differential cross section at larger values of $\tau = E\theta$. Francois *et al.*[3] measured differential-charge-exchange cross sections as well as the elastic and inelastic differential cross sections. After the measurements were also normalized to the theoretical curve at $\tau = 4$ keV deg, Francois *et al.* obtained a very good fit to the theoretical curve for the total differential cross section when the differential-charge-exchange cross section was added to the elastic

and inelastic differential cross sections.

When we made similar comparisons by using our absolute elastic and inelastic data, we observed that they fit the theoretical curve at low values of τ and that our values of ρ fell below the theoretical curve at higher values of τ. To make a more valid comparison with the theory, we measured the differential-charge-exchange cross section at 25 keV. We made the measurement by introducing a particle multiplier in the "straight-through" port of the magnet, which is behind the collision chamber. Neutral Li^0 atoms, which are scattered into the system's acceptance geometry, are undeviated by the magnet and strike the first stage of the multiplier. The Li^+ ions, which are scattered into the acceptance geometry, are steered by the magnet into the decelerator-energy analyzer-detector system. The result was not entirely satisfactory, because we were not able to calibrate the particle multiplier so that the results were consistent with earlier calibrations. The relative differential-charge-exchange measurements were, therefore, normalized to the total-charge-exchange measurement of Allison *et al.*[15] The elastic, inelastic, and charge-exchange differential cross sections were then summed to give a "total" differential cross section.

Figure 2 shows a ρ-vs-τ plot for 25-keV Li^+ ions incident on He. The reduced cross section ρ in this plot is the sum of the elastic 20- and 60-eV energy-loss inelastic and charge exchange cross sections. In this measurement, the elastic and inelastic cross sections are absolute, and the charge-exchange measurement was normalized as mentioned above. The experimental points are about 35% below the theoretical curve[14,16] and lie roughly parallel to the curve. Because both of the low-energy measurements were normalized to the theory, the lack of agreement on magnitude is not necessarily an indication that our measurements are low. It should also be noted that ρ still does not include cross sections for all excitation processes. While the differential ionization cross section is not large, it is not negligible. Anderson *et al.*[17] estimate from their optical measurements that the excitation of the S, P, and D levels for $n > 2$ is $\approx 5\%$ of the 20-eV inelastic cross section. The agreement with theory is very good if one considers the experimental uncertainties and the fact that some contributions to ρ are missing.

Figure 3 shows a ρ-vs-τ plot for the elastic scattering of Li^+ ions by He. The data are not normalized to any other experiment or theory. Because the noise is more or less constant, measurements at low intensity are much more uncertain, and the values of $\rho = \theta \sin\theta \, d\sigma/d\Omega$ at large angles are more uncertain even if their magnitudes are equal to values at smaller angles. Measurements of $\tau = E\theta$ become increasingly uncertain at the higher energies because the uncertainty of the angular measurement is multiplied by the energy.

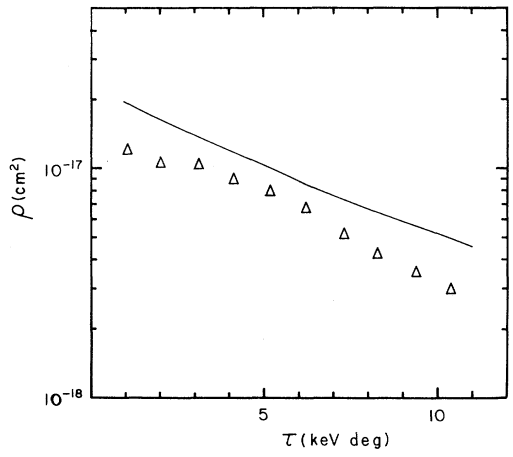

FIG. 2. Apparent reduced cross section $\rho = \theta \sin\theta \, d\sigma/d\Omega$ for 25-keV Li^+ + He collisions. The data points include the sum of our elastic 20-eV energy-loss and 60-eV energy-loss cross sections and charge-exchange differential cross sections. The elastic and inelastic measurements are absolute; the charge-exchange cross sections have been normalized to the data of Allison *et al.* (Ref. 15). The data points do not include contributions from excitation of the target to states higher than $n = 2$ or ionization. The solid line is the theoretical calculation of Catlow *et al.* (Ref. 14).

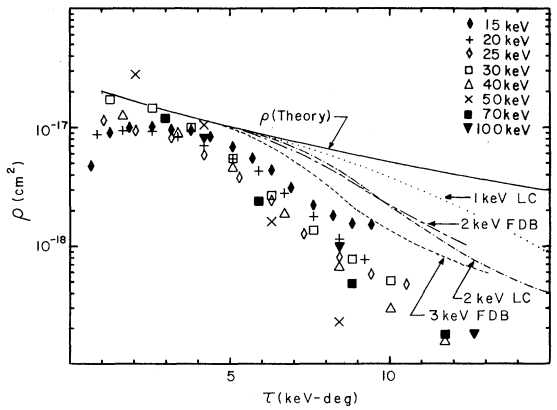

FIG. 3. Apparent reduced-cross-section measurements for elastic scattering $\rho = \theta \sin\theta \, d\sigma/d\Omega$ vs $\tau = E\theta$. ρ, τ, and θ are expressed in center-of-mass coordinates, but the identifying energies are given in laboratory coordinates. Curves labeled LC are the data of Lorents and Conklin (Ref. 1); curves labeled FDB are the data of Francois *et al.* (Ref. 3). The solid curve labeled theory is the calculation of Catlow *et al.* (Ref. 14).

The data of Lorents and Conklin[1] and of Francois *et al.*[3] were normalized to the theoretical calculation of Catlow *et al.*[14] These low-energy data seem to have slightly higher values and less slope than those derived from our measurements. If one considers the differences in energy, technique, and normalization, the similarities in the curves are more striking than the differences. All of the data exhibit curves of similar shape and decrease somewhat more rapidly with large values of τ as the ion energy increases. The differences in magnitude are small in relation to the large range in energy.

The data for the 21- and 60-eV peaks do not exhibit this behavior. The maximum in the ρ-vs-τ plots for these transitions moves to lower τ with increasing energy. The possibility of a velocity dependence in R, the radius at which the proposed curve crossings occur, was noted by Lorents and Conklin.[1] This effect and the implications of the constant ratios of He($2\,^1S$) to He($2\,^1P$) excitations in the 21-eV peak have been discussed by Park *et al.*[4] The velocity dependence of the cross sections is even more noticeable in the ρ-vs-τ plots for the 60-eV peak. The curves rise sharply and seem to break abruptly to an almost constant value for ρ. The same behavior is also noted in the curves of Lorents and Conklin[1] and of Francois *et al.*[3] where the value of τ, at which the break occurs, shows an obvious monotonic decrease with increasing energy across the entire energy span from 1 to 100 keV. With the exception of the location of the peak in the curves, the current high-energy curves and those observed by Francois *et al.*[3] and Lorents and Conklin[1] look very much alike.

The calculations of Olson[18] indicate that plots of $\rho = \theta \sin\theta (d\sigma/d\Omega)$ vs $E^{3/2}\theta$ provide a reduced plot for collisions involving a rotational coupling. Figure 4 shows our data for the 20-eV peak and the low-energy data of Lorents and Conklin[1] and that of Francois *et al.*[3] in a ρ-vs-$E^{3/2}\theta$ plot. As Olson[18] predicted, many of the threshold effects have been removed and the velocity dependence has been largely accommodated. The magnitude of ρ at the peak in the curve is not expected to be exactly identical over the entire energy range even if the threshold effects are removed by the ρ-vs-$E^{3/2}\theta$ plot, because the branching ratio between the excitation and charge exchange channel depends on the velocity.[16] However, a common curve could be drawn through the points, which would provide within a factor of 2 a representation of the data covering the entire energy range. This variation in magnitude is more noticeable in the 60-eV data shown in Fig. 5. The ρ-vs-$E^{3/2}\theta$ plot for the 60-eV energy-loss peak also provides a much improved representation of the data. The curves all rise steeply at about the same value of $E^{3/2}\theta$. Again, it would be relatively straightforward to design a common curve with an energy dependent multiplier. It would be very interesting to have differential charge exchange data available for the competing channels to determine if the changing magnitude is due to the rotational coupling mechanism or entirely to changes of branching ratios.

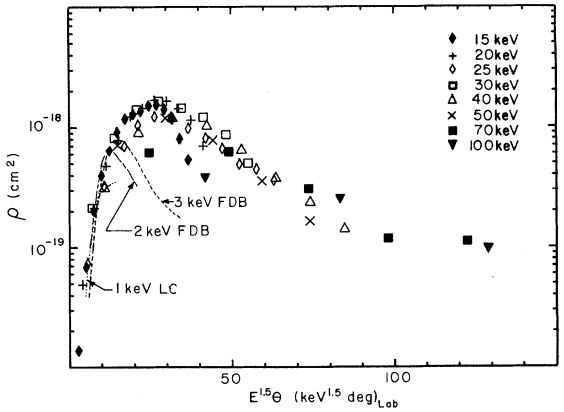

FIG. 4. Apparent reduced-cross-section measurements for excitation of the 20-eV peak $\rho = \theta \sin\theta\, d\sigma/d\Omega$ vs $E^{1.5}\theta$. The term ρ is expressed in center-of-mass coordinates while the identifying ion energies and $E^{1.5}\theta$ are expressed in laboratory coordinates. The curve labeled LC is derived from the data of Lorents and Conklin (Ref. 1). The curve labeled FDB is from the data of Francois *et al.* (Ref. 3).

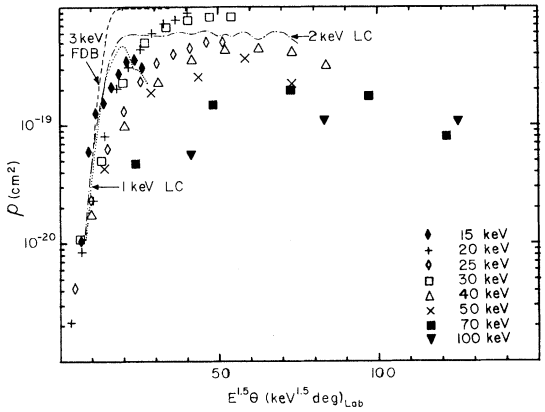

FIG. 5. Apparent reduced-cross-section measurements for excitation of the 60-eV energy-loss peak $\rho = \theta \sin\theta\, d\sigma/d\Omega$ vs $E^{1.5}\theta$. The term ρ is expressed in center-of-mass coordinates while the identifying ion energies and $E^{1.5}\theta$ are expressed in laboratory coordinates. The curve labeled LC is derived from the data of Lorents and Conklin (Ref. 1). The curve labeled FDB is from the data of Francois *et al.* (Ref. 3).

In any case, the differences in the curves are small with regard to the large energy range involved.

The data included in this article, together with previous low-energy data, provide a complete and consistent set of elastic and inelastic-differential-collision cross-section measurements that cover the energy range from 1 to 100 keV. Use of curves taken from the ρ-vs-$E^{3/2}\theta$ plots will permit accurate extrapolation of existing data to other energies. The data show remarkable consistency in the general features of both the elastic and inelastic differential cross sections over the 1- to 100-keV energy range.

ACKNOWLEDGMENTS

We are very grateful to R. E. Olson for allowing us to use the results of his preliminary calculations prior to publication. We also thank F. T. Smith for bringing this recent work to our attention.

---

†Work supported by the National Science Foundation.

*Present address: Physics Department, University of Windsor, Ontario, Canada.

‡Present address: Physics Department, University of Wisconsin, Madison, Wisc. 53706.

[1]D. C. Lorents and G. M. Conklin, J. Phys. B 5, 950 (1972).

[2]R. McCarroll and R. D. Piacentini, J. Phys. B 5, 973 (1972).

[3]R. Francois, D. Dhuicq, and M. Barat, J. Phys. B 5, 963 (1972).

[4]J. T. Park, V. Pol, J. Lawler, and J. George, Phys. Rev. Lett. 30, 1013 (1973).

[5]V. Pol. W. Kauppila and J. T. Park, Phys. Rev. A 8, 2990 (1973).

[6]J. T. Park and F. D. Schowengerdt, Rev. Sci. Instrum. 40, 753 (1969).

[7]D. R. Schoonover and J. T. Park, Phys. Rev. A 3, 228 (1971).

[8]G. W. York, J. T. Park, J. J. Miskinis, D. H. Crandall, and V. Pol, Rev. Sci. Instrum. 43, 230 (1972).

[9]O. Heinz and R. T. Reaves, Rev. Sci. Instrum. 39, 1229 (1968).

[10]G. W. York, J. T. Park, V. Pol, and D. H. Crandall, Phys. Rev. A 6, 1497 (1972).

[11]H. A. Bethe, Phys. Rev. 89, 1256 (1953).

[12]M. Barat, J. Baudon, and A. Septier, C. R. Acad. Sci. (Paris) 259, 2397 (1964).

[13]M. Boersch, G. Forst, and S. Schweda, Z. Phys. 174, 446 (1963).

[14]G. W. Catlow, M. R. C. McDowell, J. J. Kaufman, K. M. Sachs, and E. S. Chang, J. Phys. B 3, 833 (1970).

[15]S. K. Allison, J. Cuevas, and M. Garcia-Munoz, Phys. Rev. 120, 1266 (1960).

[16]C. Lesech, R. McCarroll, and J. Baudon, J. Phys. B 6, L11 (1973).

[17]N. Anderson, K. Jensen, E. Veje, and O. Nielson, Z. Phys. 264, 349 (1973).

[18]R. Olson, Stanford Research Institute (private communication).